Skin-specific regulation of SREBP processing and lipid biosynthesis by glycerol kinase 5

Duanwu Zhang[a], Wataru Tomisato[a,1], Lijing Su[a], Lei Sun[a], Jin Huk Choi[a], Zhao Zhang[a], Kuan-wen Wang[a], Xiaoming Zhan[a], Mihwa Choi[a], Xiaohong Li[a], Miao Tang[a], Jose M. Castro-Perez[b,2], Sara Hildebrand[a], Anne R. Murray[a], Eva Marie Y. Moresco[a], and Bruce Beutler[a,3]

[a]Center for the Genetics of Host Defense, University of Texas Southwestern Medical Center, Dallas, TX 75390-8505; and [b]Merck & Co., Inc., Kenilworth, NJ 07033

Contributed by Bruce Beutler, May 9, 2017 (sent for review March 30, 2017; reviewed by Daniel L. Kastner and Christos C. Zouboulis)

The recessive *N*-ethyl-*N*-nitrosourea–induced phenotype *toku* is characterized by delayed hair growth, progressive hair loss, and excessive accumulation of dermal cholesterol, triglycerides, and ceramides. The *toku* phenotype was attributed to a null allele of *Gk5*, encoding glycerol kinase 5 (GK5), a skin-specific kinase expressed predominantly in sebaceous glands. GK5 formed a complex with the sterol regulatory element-binding proteins (SREBPs) through their C-terminal regulatory domains, inhibiting SREBP processing and activation. In $Gk5^{toku/toku}$ mice, transcriptionally active SREBPs accumulated in the skin, but not in the liver; they were localized to the nucleus and led to elevated lipid synthesis and subsequent hair growth defects. Similar defective hair growth was observed in kinase-inactive GK5 mutant mice. Hair growth defects of homozygous *toku* mice were partially rescued by treatment with the HMG-CoA reductase inhibitor simvastatin. GK5 exists as part of a skin-specific regulatory mechanism for cholesterol biosynthesis, independent of cholesterol regulation elsewhere in the body.

alopecia | glycerol kinase | sebocyte | cholesterol biosynthesis | SREBP

Cholesterol is an essential structural component of the vertebrate cell membrane as well as a precursor of steroid hormones, vitamins, and bile acids (1). Biosynthesis of cholesterol and other lipids in the skin is essential for the formation of the epidermal permeability barrier, for hair follicle morphogenesis, and for hair follicle maintenance (2–8). Sebaceous glands and epidermal keratinocytes are the two major sources of skin lipid production (9). Sebocytes are terminally differentiated epithelial cells of sebaceous glands that produce and secrete sebum, a lipid mixture composed of triglycerides and fatty acids (57.5%), wax esters (26%), squalene (12%), and cholesterol (4.5%) (10). Sebum provides protection against bacterial infections, prevents moisture evaporation, and promotes normal hair follicle differentiation and cycling (11–14).

On the other hand, cholesterol and fatty acids can be toxic to cells, which must regulate their production to avoid overaccumulation (15). Sterol regulatory element-binding proteins (SREBPs), members of the basic-helix–loop–helix leucine zipper (bHLH-zip) class of transcription factors, are required for de novo cholesterol, fatty acid, and triglyceride biosynthesis (16). Nearly all genes encoding cholesterol synthesis enzymes are SREBP targets (17). In humans, there are two SREBP genes, *SREBF1* and *SREBF2*. *SREBF1* encodes SREBP-1a and SREBP-1c, which possess different first exons through the use of an alternative promoter, whereas *SREBF2* encodes a single protein product, SREBP-2 (18). SREBP-1a and SREBP-2 are constitutively expressed in most tissues, whereas SREBP-1c expression is induced in response to changes in diet and insulin levels (19, 20). SREBP-1a and SREBP-1c are more active in driving the transcription of genes involved in fatty acid synthesis, whereas SREBP-2 is more active in driving the transcription of genes involved in cholesterol biosynthesis (21, 22).

Under conditions of sterol sufficiency, SREBPs are retained in the endoplasmic reticulum (ER) by formation of a complex with the cholesterol-sensing SREBP cleavage-activating protein (SCAP) and the ER-resident membrane protein Insig (23, 24). During conditions of sterol attenuation in the cell, the SREBP/SCAP complex is released from Insig and transported to the Golgi apparatus, where the SREBPs are sequentially cleaved by site-1 protease (S1P) and site-2 protease (S2P) to liberate their water-soluble, transcriptionally active N-terminal domains (25). Each N-terminal domain is then translocated into the nucleus where it binds to sterol regulatory element DNA sequences to promote the transcription of genes encoding enzymes required for sterol biosynthesis (26, 27).

Here, we investigated the mechanisms underlying progressive alopecia observed in *Gk5*-deficient mice. Our findings suggest that an excess of cholesterol or its precursors disrupts hair follicle development and cycling in these animals.

Results

Alopecia Caused by a Recessive Mutation of *Gk5*. We observed a mouse with alopecia among the third generation (G3) of C57BL/6J mice carrying mutations induced by *N*-ethyl-*N*-nitrosourea (ENU) (Fig. 1*A*); no other visible abnormalities were observed. The phenotype, called *toku*, was transmissible as an autosomal recessive trait in the expected Mendelian ratio and was expressed by both male and female offspring.

Significance

We discovered a previously unrecognized regulator of cholesterol biosynthesis, glycerol kinase 5 (GK5), which functions exclusively in the skin independently of cholesterol regulation in other tissues. GK5 negatively regulates the processing and nuclear localization of sterol regulatory element binding proteins, transcription factors that control expression of virtually all cholesterol synthesis enzymes. Excessive amounts of cholesterol, triglycerides, and ceramides were found in the skin of GK5-deficient mice. These mice displayed alopecia (hair loss) caused by impaired hair growth and maintenance, for which proper amounts of cholesterol and other skin lipids are necessary.

Author contributions: D.Z., W.T., X.Z., and B.B. designed research; D.Z., W.T., L. Su, L. Sun, J.H.C., Z.Z., K.-w.W., X.Z., M.C., X.L., M.T., and J.M.C.-P. performed research; D.Z., W.T., X.Z., J.M.C.-P., S.H., and B.B. analyzed data; and D.Z., A.R.M., E.M.Y.M., and B.B. wrote the paper.

Reviewers: D.L.K., National Institutes of Health; and C.C.Z., Theodor Fontane Medical University of Brandenburg, Dessau Medical Center.

The authors declare no conflict of interest.

[1]Present address: Group II, Frontier Research Laboratories, R&D Division, Daiichi Sankyo Co., Ltd., Shinagawa-ku, Tokyo 140-8710, Japan.

[2]Present address: Waters Corporation, Milford, MA 01757.

[3]To whom correspondence should be addressed. Email: bruce.beutler@UTSouthwestern.edu.

This article contains supporting information online at www.pnas.org/lookup/suppl/doi:10.1073/pnas.1705312114/-/DCSupplemental.

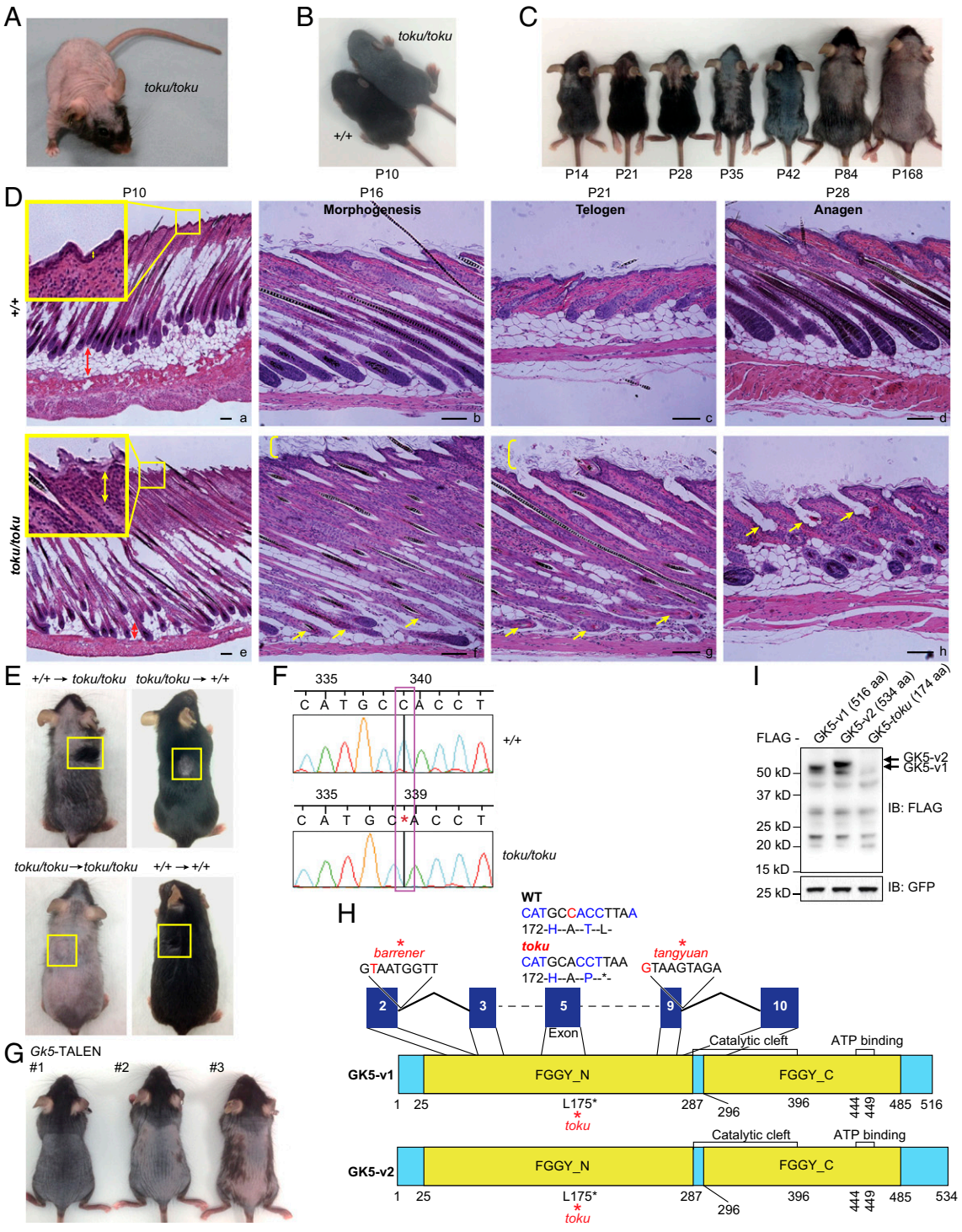

Fig. 1. The *toku* phenotype results from a mutation in *Gk5*. (*A*) Representative adult homozygote *toku* mouse exhibiting alopecia. (*B*) Delayed hair growth in a representative *toku* homozygote (*Top Right*) at P10; a littermate wild-type mouse is shown at the *Bottom Left*. (*C*) *Toku* homozygotes exhibit hair loss that progresses with age beginning as early as P14; representative *toku* mouse is shown for each time point. (*D*) Hair follicle morphogenesis and cycling in wild-type ($^{+/+}$) and *toku* homozygotes. Upper back skin from mice of the indicated ages was fixed, sectioned longitudinally to the hair shaft, and stained with H&E. Representative sections from wild-type (a–d) or *toku* homozygous mice (e–h) were imaged at 40× (a and e) or 100× magnification (b–d, f–h). *Insets* are enlargements of the boxed areas. (Scale bars, 100 μm.) (*E*) Skin grafted from a wild-type mouse onto a homozygous *toku* mouse and from a homozygous *toku* mouse onto a wild-type mouse 35 d posttransplantation. Skin grafted from a wild-type mouse onto a wild-type mouse and from a homozygous *toku* mouse onto a homozygous *toku* mouse were included as controls. All of the images shown are representatives from at least three repeated experiments. (*F*) DNA sequence chromatogram of the deleted nucleotide in *Gk5*. (*G*) The phenotype of three Gk5-TALEN founders. The DNA sequence of each of the TALEN-induced mutations in the founders is shown in Fig. S2C. (*H*) Domain structures of isoform 1 (GK5-v1) and isoform 2 (GK5-v2) of mouse GK5. The putative locations of the FGGY_N, FGGY_C, catalytic cleft, and ATP-binding domains, as predicted by SMART and UniProt, are indicated. The locations of the *toku*, *barrener*, and *tangyuan* mutations are indicated in GK5-v1; the mutations affect similar regions in both isoforms. The *barrener* and *tangyuan* mutations affect splice donor sites. (*I*) Immunoblot analysis of exogenously expressed FLAG-tagged GK5-v1, FLAG-tagged GK-v2, and a truncated FLAG-tagged GK5 (GK5-*toku*; amino acids 1–174) from HEK293T cells using antibodies against FLAG and GFP. GFP was probed as a transfection efficiency control.

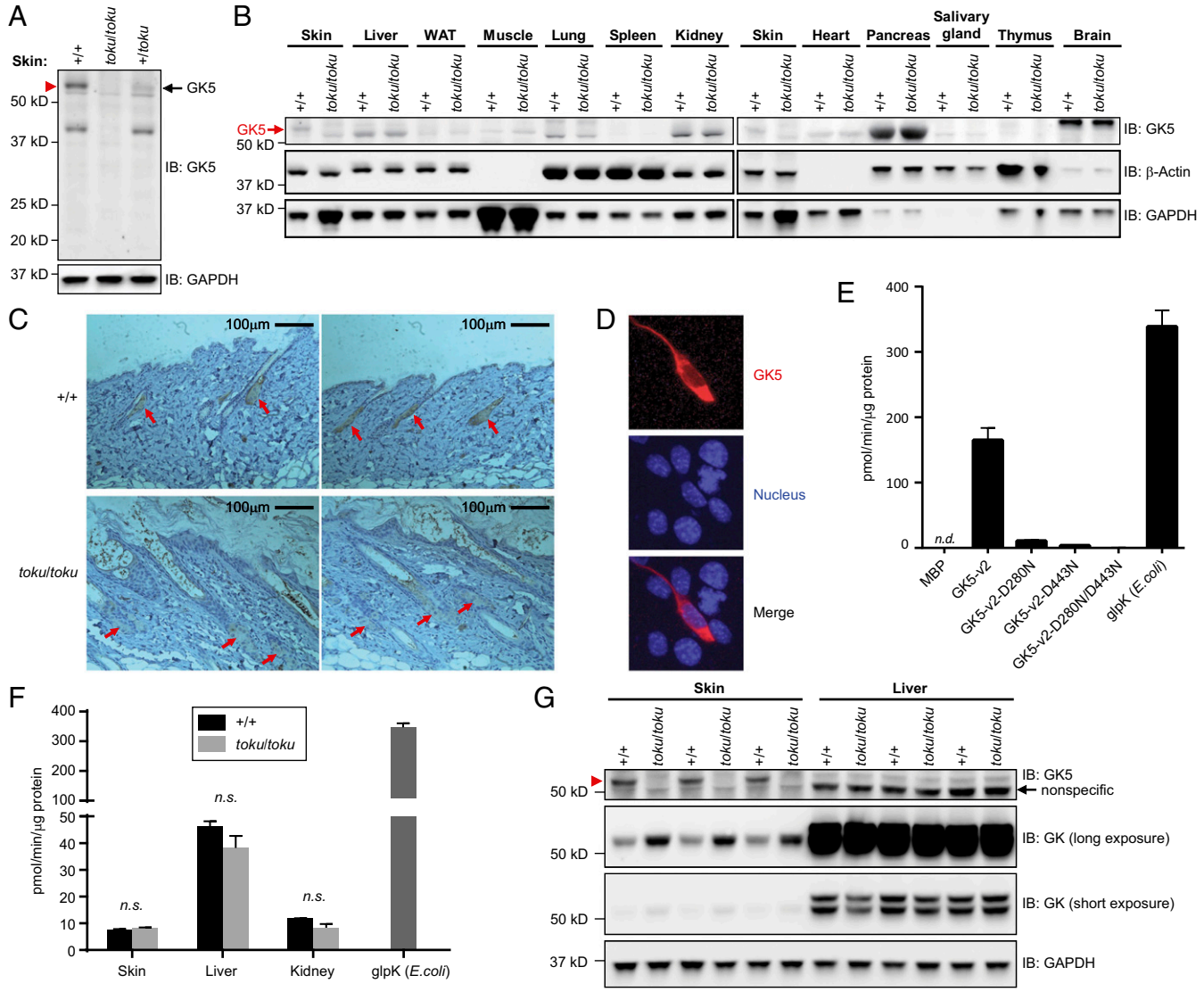

Fig. 2. GK5 is predominantly expressed in the sebaceous glands of the skin and exhibits glycerol kinase activity. (*A*) Skin lysates from wild-type ($^{+/+}$), *toku* heterozygote (+/*toku*), and *toku* homozygote (*toku*/*toku*) mice were immunoblotted using antibodies against GK5 and GAPDH. GAPDH was the loading control. (*B*) Lysates from skin, liver, white adipose tissue (WAT), muscle, lung, spleen, kidney, heart, pancreas, salivary gland, thymus, and brain from wild-type and *toku* homozygotes were immunoblotted using the indicated antibodies. β-Actin and GAPDH were the loading controls. (*C*) Immunohistochemical staining of P56 skin sections shows that GK5 is expressed mainly in the sebaceous glands in wild-type mouse skin; GK5 was not detected in the *toku* skin. Images were captured at 200× magnification. (Scale bar, 100 μm.) Representative images are shown. (*D*) FLAG-tagged GK5-v2 localized mainly in the cytoplasm in transfected NIH 3T3 cells. Immunofluorescence was performed using the FLAG antibody. DAPI stained the nuclei of the cells. All of the experiments were repeated at least three times, and a representative experiment is shown. (*E*) Glycerol kinase activity (pmol/min/μg) of recombinant wild-type GK5 or GK5 with one or both of the point mutations D280N and D443N. A coupling rate of 0.436 based on the manufacturer's instruction was used to calculate the specific activities. Recombinant *E. coli* glycerol kinase (glpK; R&D Systems) is the positive control for the assay. Data represent means ± SD. (*F*) Total glycerol kinase activity (pmol/min/μg) in skin, liver, and kidney of wild-type and *toku* homozygotes. Recombinant glpK was used as a positive control. Data represent means ± SD. (*G*) Lysates from skin and liver from wild-type and *toku* homozygotes were immunoblotted using antibodies against GK5, GK, and GAPDH. GAPDH is the internal control.

During the onset of initial hair growth, *toku* homozygotes exhibited delayed eruption of hair from the skin surface (Fig. 1*B*). During the catagen/telogen phase of the first hair cycle [approximately postnatal day (P)16–P19 in the mouse], *toku* homozygotes exhibited less hair growth compared with wild-type and *toku* heterozygous mice and displayed dorsal hair loss (Fig. 1*C*). Hair length and texture were comparable in *toku* homozygotes and wild-type mice. Hair loss in *toku* homozygotes continued through the anagen (~P21–P30) phase of the first hair cycle. By the telogen phase (~P30–P70), *toku* homozygotes had severe dorsal hair loss that continued to progress so that by 24 wk of age they exhibited almost complete hair loss (Fig. 1*C*). These results indicated that proliferation and/or differentiation defects of *toku* hair follicles halt progression through additional cycles after the first hair follicle cycle.

To characterize the hair follicle defects of *toku* homozygotes, histological sections of skin from wild-type and *toku* homozygotes were compared. At P10, the hair follicles of the wild-type mice aligned normally (Fig. 1 *D*, a), whereas those of the *toku* homozygotes were less regular in their alignment (Fig. 1 *D*, e). Epidermal hyperplasia (see yellow boxes in Fig. 1 *D*, e) and a loss of hypodermal adipocytes were also evident (Fig. 1 *D*, e and Fig. S1*A*). At P16, near the end of follicular morphogenesis, the hair follicles of the *toku* homozygotes exhibited degeneration of the hair bulb, and the *toku* skin started to exhibit hyperkeratosis (Fig.

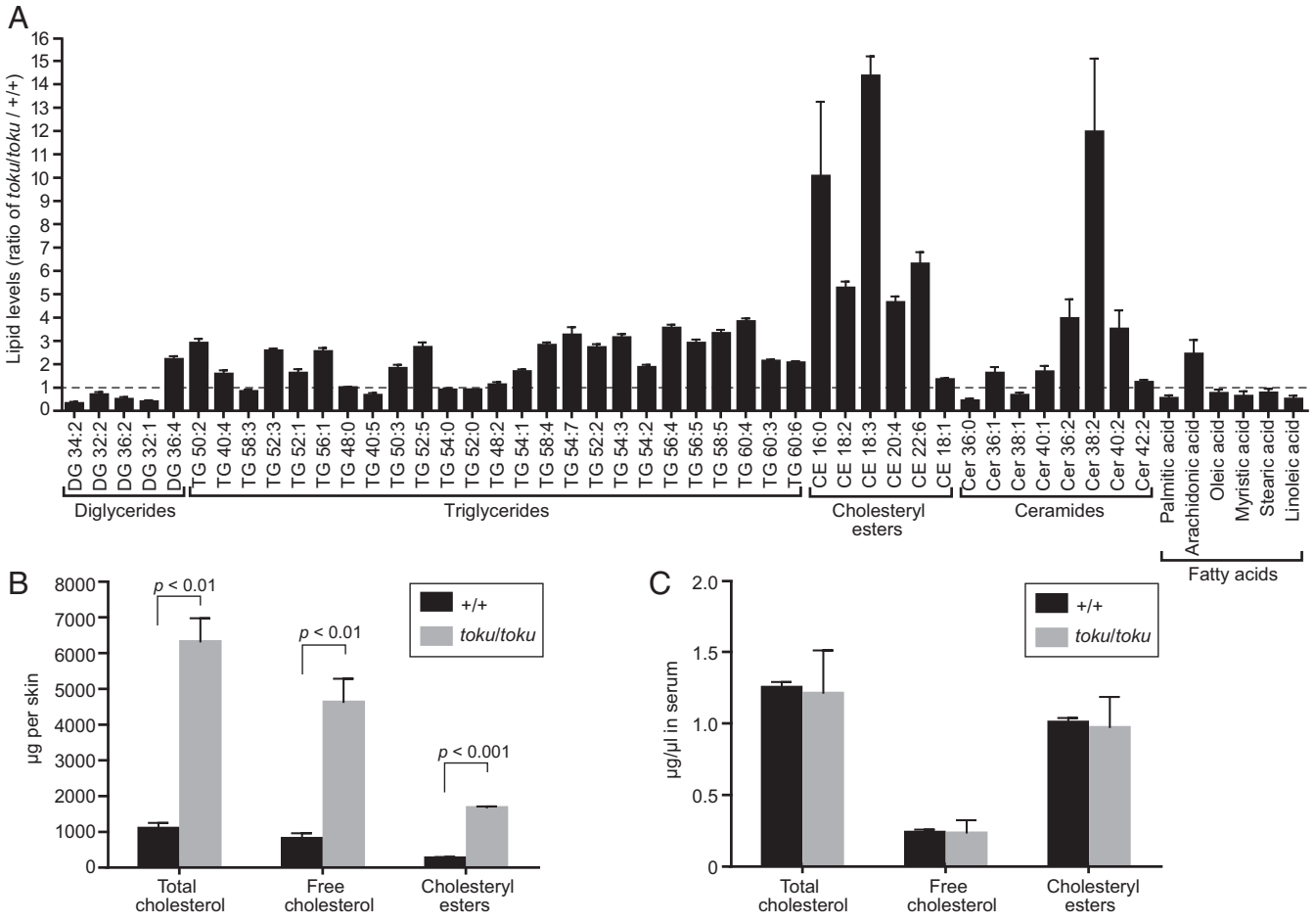

Fig. 3. *Gk5* deficiency causes increased cholesterols in the skin of *toku* homozygotes. (*A*) Skin lipid profile in the *toku* homozygotes. Values were obtained by LC/MS and are graphed as the ratio of lipid amounts in the *toku* skin ($n = 5$) to the equivalent lipids in wild-type mice ($n = 5$). Data represent means ± SD. (*B*) Amounts (µg per skin) of free cholesterol, cholesteryl esters, or both (total cholesterol) in the skin of *toku* ($n = 3$) and wild-type mice ($n = 3$). Data represent means ± SD. (*C*) Amounts (µg/µL) of free cholesterol, cholesteryl esters, or both (total cholesterol) in the serum of *toku* ($n = 3$) and wild-type mice ($n = 3$). Data represent means ± SD.

1 *D*, f). At P21, follicular cycling was arrested in *toku* homozygotes, hyperkeratosis persisted, and degeneration was observed along the length of the hair follicles (Fig. 1 *D*, g). At P28, as the hair follicles of the wild-type mice proceeded into anagen phase (Fig. 1 *D*, d), the hair follicles of the *toku* homozygotes had completely degenerated and did not proceed to anagen phase (Fig. 1 *D*, h). Hence, alopecia in the *toku* homozygotes resulted from defective hair follicle morphogenesis and maintenance, impaired progression through the hair cycle, and eventual degeneration of the hair follicle. Notably, we also observed abnormalities of keratinocyte differentiation in the three epidermal layers of homozygous *toku* skin (Fig. S1 *B* and *C*).

To determine whether the *toku* alopecia phenotype is due to a defect localized to the skin, reciprocal syngeneic skin transplants were performed. Shaved dorsal skin from *toku* or wild-type mice was grafted onto wild-type or *toku* homozygotes, respectively. In the wild-type mouse, *toku* grafts retained their hairless phenotype, whereas wild-type skin transplanted onto a *toku* mouse showed normal hair growth (Fig. 1*E*). These results indicated that hair growth was dependent on the skin-intrinsic function of a gene disrupted by the *toku* mutation.

The *toku* phenotype was mapped by bulk segregation analysis to a 57.4-Mbp critical region on mouse chromosome 9 (Fig. S2*A*). Fine mapping narrowed the proximal and distal boundaries of the critical region to 6.8 Mbp (92,626,213–99,422,251 bp), containing 38 protein-coding genes. Among the candidate genes, *Esyt3* (extended synaptotagmin-like protein 3) and *Gk5* were selected for Sanger sequencing due to high expression levels in mouse epidermis [BioGPS; Dataset: GeneAtlas MOE430, gcrma (28)]. We identified a deletion of a cytosine (C) at base pair 96,140,631 (NCBI v38) on chromosome 9 within exon 5 of *Gk5* in the *toku* mice (Fig. 1*F*). Whole-exome sequencing of all coding exons and splice junctions in a homozygous *toku* mouse confirmed that *Gk5* was the only affected gene on chromosome 9 (Fig. S2*B*). Three *Gk5*-deficient mouse strains generated by transcription activator-like effector nuclease (TALEN)-mediated gene targeting (Fig. 1*G* and Fig. S2*C*) and two additional ENU-induced mutants (named *tangyuan* and *barrener*) carrying null alleles of *Gk5* exhibited progressive hair loss (Fig. 1*H* and Fig. S2 *D* and *E*), confirming that the *toku* phenotype is caused by *Gk5* mutations.

Gk5 has two predicted splice variants that encode a 516-aa (GK5-v1) and a 534-aa (GK5-v2) protein product (Ensembl: ENSMUSP00000112717 and ENSMUSP00000082313, respectively) that differ in sequence and length after amino acid 515 (Fig. 1*H*). Both variants were successfully cloned from mouse cDNA, demonstrating that both are expressed in the mouse; however, overexpression in HEK293T cells suggested that GK5-v1 is less stable than GK5-v2 (Fig. 1*I*). The *toku* mutation occurs at base pair 595 within both *Gk5* transcripts, causing a frameshift that encodes one novel amino acid followed by a premature stop after amino acid 174 (Fig. 1*H*). Exogenous expression of GK5^{toku}

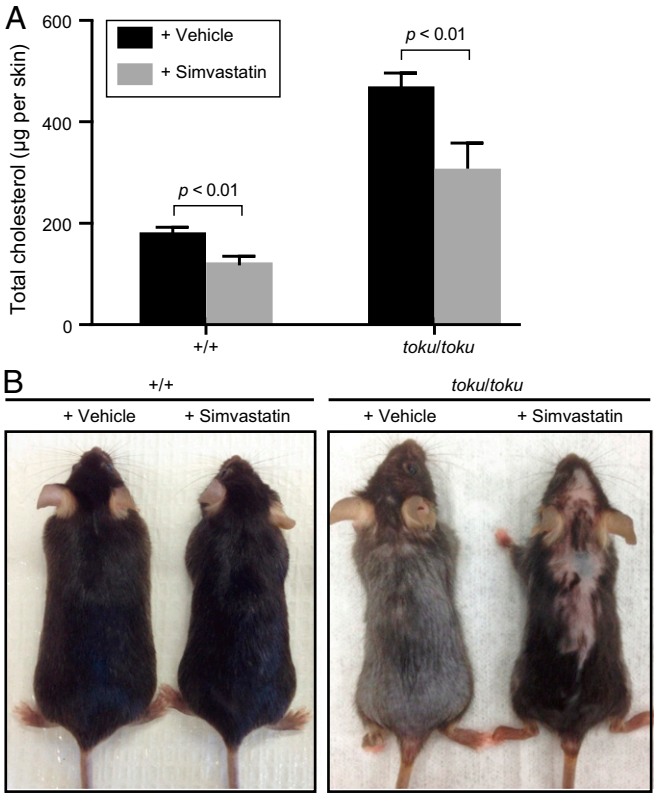

Fig. 4. Alopecia phenotype of *toku* mice is corrected by simvastatin treatment. (*A*) Wild-type and *toku* homozygotes were treated with either vehicle only or vehicle plus simvastatin from P2 to P14. The amount (μg) of total cholesterol in each skin was measured at P15. Data represent means ± SD of three independent experiments. (*B*) Simvastatin treatment as described in *A*. Images were captured at P90. Representative images are shown.

in HEK293T cells revealed that the truncated GK5^{toku} protein product was unstable (Fig. 1*I*).

GK5 Is a Sebocyte-Specific Protein That Exhibits Glycerol Kinase Activity. Using a polyclonal antibody against the N terminus of GK5, immunoblot analysis of whole-skin lysates from wild-type (+/+), *toku* heterozygote (+/*toku*), and *toku* homozygote (*toku*/*toku*) mice revealed a single band of ∼60 kDa corresponding in size to GK5-v2 in wild-type and *toku* heterozygote skin, but not in *toku* homozygote skin (Fig. 2*A*). Although *Gk5* mRNA was detected in numerous tissues (Fig. S3*A*), a single 60-kDa GK5 band was present in wild-type skin but not in other tissues tested (Fig. 2*B*). Immunostaining of wild-type dorsal skin sections demonstrated localization of GK5 to the sebaceous glands adjacent to the hair follicle (Fig. 2*C*). Immunostaining of GK5-transfected NIH 3T3 cells showed that GK5 was confined mainly to the cytoplasm (Fig. 2*D*).

To determine whether GK5 harbors glycerol kinase activity, recombinant GK5 was purified as a maltose-binding protein (MBP)-fusion protein, and then the MBP tag was removed by cleavage with tobacco etch virus (TEV) protease. Glycerol kinase activity was determined by measuring the ability of the purified GK5 to transfer phosphate from ATP to glycerol. The specific activity of recombinant GK5 was 153 pmol/min/μg protein, which was dramatically reduced by the point mutations D280N or D443N and abolished by a combination of the two mutations (Fig. 2*E*). The specific activity of GK5 was lower than that of commercial recombinant *Escherichia coli* GK (glpK; 340 pmol/min/μg protein). Total glycerol kinase activity in the skin as well as liver and kidney (Fig. 2*F*), which were sites of high *Gk* expression (Fig. S3*B*), was not significantly different between the *toku* homozygotes and wild-type mice.

We tested the importance of GK5 kinase activity for normal hair growth using mice carrying a kinase-inactivating point mutation of GK5 (D280N) generated by CRISPR-Cas9 gene targeting. Despite normal or slightly elevated expression of kinase-inactive GK5 (Fig. S4*A*), homozygous mutants (*Gk5*$^{D280N/D280N}$) exhibited hair loss similar to that observed in *toku* homozygotes or TALEN-induced *Gk5*$^{-/-}$ mice (Fig. S4*B*), indicating that GK5 kinase activity is necessary for normal hair growth.

The GK family has three members: GK, GK2, and GK5. Because total glycerol kinase activity was comparable in the skin of *toku* and wild-type mice, we examined the expression levels of the other GK family members for compensatory up-regulation in *toku* skin. GK protein expression was increased in *toku* skin, but not in liver, compared with wild-type expression levels (Fig. 2*G*). The expression level of *Gk2* mRNA in the skin and liver of *toku* mice was unchanged with respect to that observed in wild-type mice (Fig. S5*A*), and CRISPR-Cas9–targeted *Gk2*$^{-/-}$ mice did not exhibit hair loss (Fig. S5 *B* and *C*).

GK5 Deficiency Causes Increased Cholesterol, Triglyceride, and Ceramide Levels in the Skin. Changes in lipid composition, including the overproduction and/or the buildup of sterol precursors of cholesterol, can lead to alterations in hair follicle development and hair loss (29). Liquid chromatography/mass spectrometry (LC/MS) was used to measure acetone-eluted diglycerides, triglycerides, cholesteryl esters, ceramides, and free fatty acids in the skin of five wild-type and five *toku* homozygous mice. The average level of each skin lipid in *toku* homozygotes was compared with the average wild-type level. Relative to wild-type skin, the skin of *toku* homozygotes contained increased levels of 34 of 50 lipids tested (Fig. 3*A*). Among them, cholesteryl esters showed the greatest increases, with five of the six cholesteryl esters demonstrating from 5- to 14-fold higher levels in *toku* skin than in wild-type skin (Fig. 3*A*). Further examination of the levels of free cholesterol, total cholesteryl esters, or both (total cholesterol) confirmed that all three were elevated in skin (Fig. 3*B*), but not in serum (Fig. 3*C*), of *toku* homozygous mice compared with wild-type mice, consistent with the proposed skin intrinsic phenotype of *toku* mice suggested by skin transplantation (Fig. 1*E*). These data demonstrate that mutation of GK5 results in elevated skin lipids, including free cholesterol, cholesteryl esters, triglycerides, and ceramides.

Rescue of *toku* Phenotype by Simvastatin. HMGCR [3-hydroxy-3-methylglutaryl (HMG)–CoA reductase] is the rate-determining enzyme of cholesterol biosynthesis that converts HMG–CoA to mevalonate (30). Simvastatin is a statin inhibitor of HMGCR that lowers levels of sterol precursors and cholesterol in the skin (31). Daily topical simvastatin treatment for 13 d (P2–P14) resulted in reduced cholesterol levels in the back skin of both the *toku* and wild-type mice at P15 (Fig. 4*A*); no appreciable hair growth was apparent on the treated mice immediately after the simvastatin treatment. Then at P90, the vehicle- and simvastatin-treated mice were photographed and hair growth was noted. Hair growth of wild-type mice was not affected by vehicle or simvastatin treatment (Fig. 4*B*; 4 of 4 total mice), and all vehicle-treated *toku* mice exhibited hair loss similar to untreated *toku* homozygotes (Fig. 4*B*; 5 of 5 total mice). However, the *toku* homozygotes treated with simvastatin exhibited partial correction of the hair loss phenotype (Fig. 4*B*; 4 of 5 total mice). These results strongly suggest that increased sterol precursors and/or cholesterol in the skin cause hair loss in *Gk5*-deficient mice. The contribution of other lipids to the *toku* phenotype has not been investigated.

GK5 Deficiency Promotes SREBP Processing and Nuclear Translocation in the Skin. SREBP-1 and SREBP-2 promote cholesterol biosynthesis and homeostasis by stimulating the transcription of

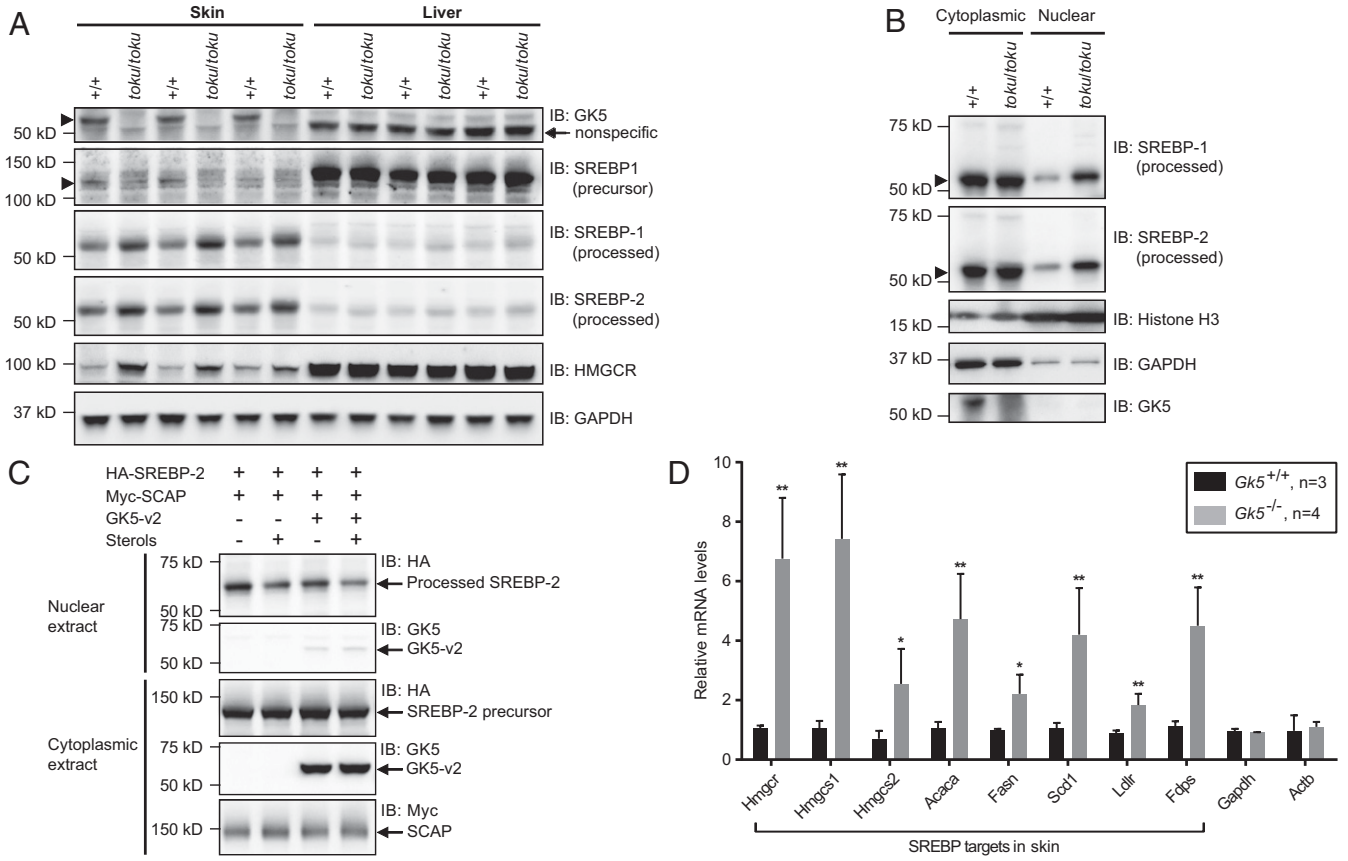

Fig. 5. GK5 deficiency promotes SREBP processing and increases the nuclear-localized transcriptionally active forms. (*A*) Immunoblot analysis of SREBP-1, SREBP-2, and their target HMGCR in the skin and liver of homozygous *toku* and wild-type mice. GAPDH is shown as the loading control. (*B*) Immunoblot analysis of SREBP-1, SREBP-2, Histone H3 (nuclear marker), GAPDH (cytoplasmic marker), and GK5 in cytoplasmic and nuclear extracts from wild-type and *toku* homozygote skin. (*C*) HEK293T cells stably expressing 3xHA-tagged SREBP-2 were transfected with Myc-tagged SCAP with or without GK5-v2. Twelve hours after transfection, cells were switched to lipoprotein-deficient medium containing 50 μM mevastatin, 50 μM mevalonate, and 1% (wt/vol) hydroxypropyl-β-cyclodextrin. After incubation for 1 h, the cells were left untreated or treated with 1 μg/mL 25-hydroxycholesterol plus 10 μg/mL cholesterol (sterols). After incubation for 8 h, cytoplasmic and nuclear extracts were prepared and immunoblotted with antibodies against HA, Myc, and GK5. (*D*) Expression levels in the skin of SREBP targets *Hmgcs1* (HMG-CoA synthase 1), *Hmgcs2* (HMG-CoA synthase 2), *Acaca* (acetyl-CoA carboxylase α), *Fasn* (fatty acid synthase), *Scd1* (stearoyl-CoA desaturase 1), *Ldlr* (low-density lipoprotein receptor), and *Fdps* (farnesyl diphosphate synthetase) were measured in wild-type ($n = 3$) and *Gk5* knockout littermates ($n = 4$). Relative mRNA levels of each are graphed. $*P < 0.05$; $**P < 0.01$.

sterol-regulated genes (32). The activities of SREBP-1 and SREBP-2 were reportedly reduced in adipose tissue from *Gk* knockout mice compared with that in wild-type mice (33). We investigated whether loss of *Gk5* function alters the expression and processing of the SREBPs in the skin and liver. Immunoblot analysis revealed that the amount of SREBP-1 precursor (125 kDa) was reduced and the amount of processed SREBP-1 (60–70 kDa) was increased in the skin of *toku* homozygotes compared with that in wild-type mice (Fig. 5*A*). In addition, the processed form of SREBP-2 (60–70 kDa) was up-regulated in skin from *toku* homozygotes compared with that in wild-type mice (Fig. 5*A*). SREBP-1 and SREBP-2 expression and processing in the livers of *toku* homozygous and wild-type mice were comparable, further supporting the skin intrinsic function of GK5 (Fig. 5*A*).

To determine whether there were changes in the localization of the processed forms of SREBP-1 and SREBP-2 in the *toku* mice, nuclear and cytoplasmic extracts were isolated from the skin. Immunoblotting revealed that the levels of the processed forms of SREBP-1 and SREBP-2 in the cytoplasm were comparable in the skin of *toku* homozygous and wild-type mice (Fig. 5*B*). However, the nuclear-localized transcriptionally active forms of SREBP-1 and SREBP-2 were increased in the skin of *toku* homozygotes compared with wild-type mice (Fig. 5*B*). Conversely, overexpression of GK5 in HEK293T cells diminished the amount of processed SREBP-2 in the nucleus that was induced by coexpression of SCAP and SREBP-2 (Fig. 5*C*); comparable levels of SREBP-2 precursor were detected in the cytoplasm with or without GK5 overexpression (Fig. 5*C*).

HMGCR is a key target of SREBP-1 and SREBP-2 (30). The level of HMGCR in the skin of the *toku* homozygotes was increased compared with that in wild-type mice, consistent with the idea that changes in HMGCR expression were leading to the increased cholesterol levels in the *toku* skin (Fig. 5*A*). The mRNA levels of other SREBP targets, including *Hmgcs1* (HMG-CoA synthase 1), *Hmgcs2* (HMG-CoA synthase 2), *Acaca* (acetyl-CoA carboxylase alpha), *Fasn* (fatty acid synthase), *Scd1* (stearoyl-CoA desaturase 1), *Ldlr* (low density lipoprotein receptor), and *Fdps* (farnesyl diphosphate synthetase) (25), were also elevated in the skin of $Gk5^{-/-}$ mice, indicating that SREBP target genes were broadly affected (Fig. 5*D*). Taken together, these data suggest that GK5 inhibits the processing of SREBP precursors to attenuate transcription of SREBP target genes.

GK5 Associates with GK, SREBP-1, and SREBP-2. Because GK expression was reported to influence SREBP-1 and SREBP-2 activity and subsequent HMGCR expression, the interaction between GK5 and GK was examined. Transient cotransfection of HEK293T cells with FLAG-tagged GK isoform 1 (FLAG-GK-v1) or isoform

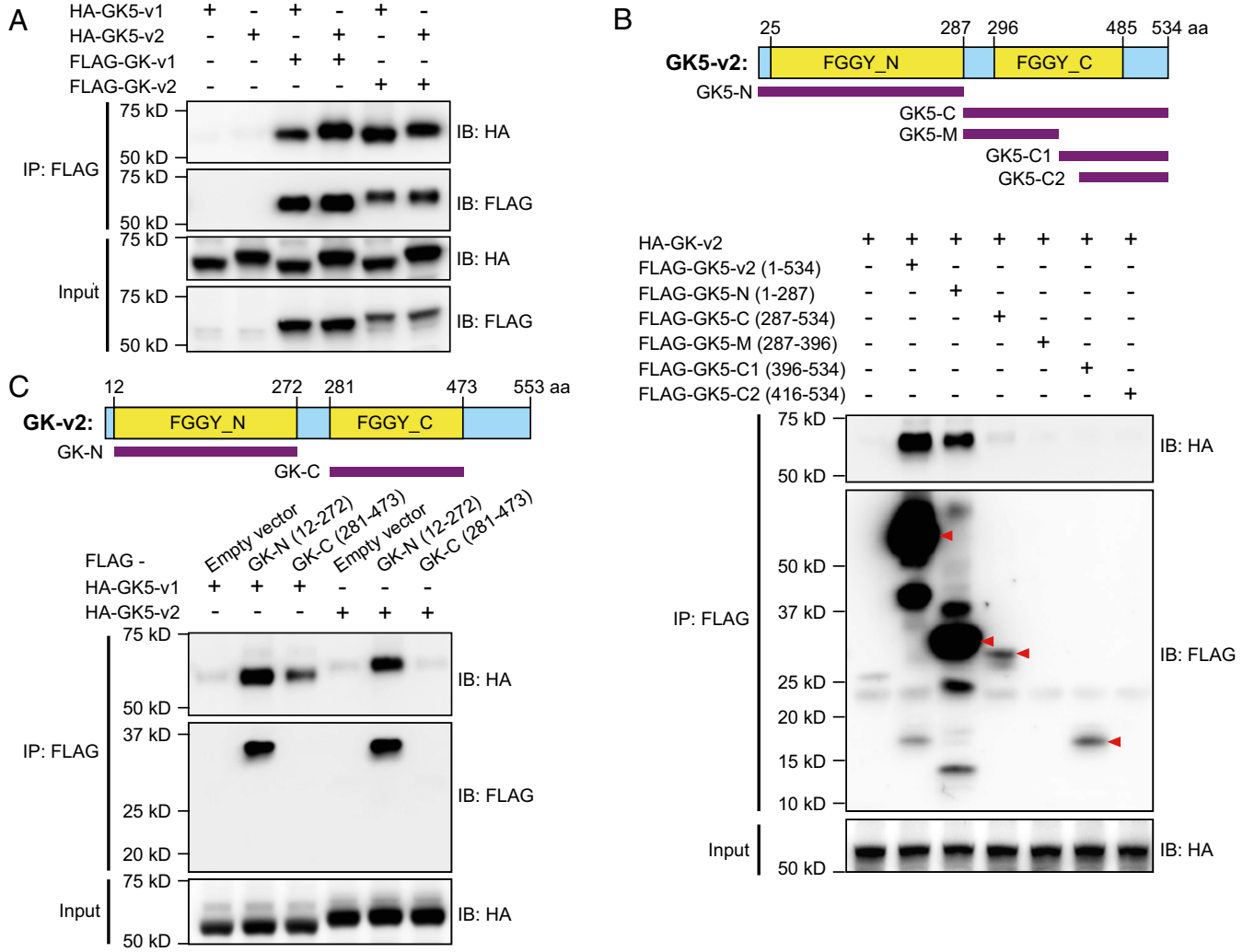

Fig. 6. GK5 associates with GK through their respective FGGY_N domains. (*A*) HEK293T cells were transfected with either FLAG-tagged GK isoform 1 (GK-v1) or isoform 2 (GK-v2) and either HA-tagged GK5-v1 or GK5-v2. Cell lysates were immunoprecipitated using anti-FLAG M2 agarose and immunoblotted with antibodies against HA and FLAG. (*B*) HEK293T cells were transfected with FLAG-tagged full-length or truncated forms of GK5-v2 and HA-tagged GK-v2. The domain structures of GK5-v2 and GK are shown. The locations of the residues used in the truncated constructs are indicated below the domain structures. Cell lysates were immunoprecipitated using anti-FLAG M2 agarose and immunoblotted with indicated antibodies. (*C*) HEK293T cells were transfected with either the FLAG-tagged FGGY_N or FGGY_C domain of GK and either HA-tagged GK5-v1 or GK5-v2. Cell lysates were immunoprecipitated using anti-FLAG M2 agarose and immunoblotted with the indicated antibodies.

2 (FLAG-GK-v2) and either HA-tagged GK5-v1 (HA-GK5-v1) or HA-GK5-v2 followed by coimmunoprecipitation and immunoblot analysis revealed that both isoforms of GK interacted with both isoforms of GK5 (Fig. 6*A* and Fig. S6*A*). Using truncated versions of GK5 and GK, we observed that the N-terminal FGGY domains of GK and GK5 were sufficient to mediate the interaction between the two proteins (Fig. 6 *B* and *C* and Fig. S6*B*), although failure of expression of the C-terminal FGGY domains of GK and GK5 precluded their analysis.

We also tested the interaction between HA-tagged GK5 or GK and either FLAG-tagged SREBP-1 or SREBP-2 in HEK293T cells. Both HA-GK5-v2 (Fig. 7*A*) and HA-GK-v2 (Fig. 7*B*) bound to FLAG-SREBP-1 and FLAG-SREBP-2. Although GK5 kinase activity was necessary for normal hair growth (Fig. S4), it was dispensable for the interaction between GK5 and SREBP-1/-2 (Fig. S7*A*). Moreover, purified recombinant GK5 failed to phosphorylate immunoprecipitated FLAG-SREBP-1/-2, which showed a basal level of phosphorylation after immunoprecipitation from HEK293 cells (Fig. S7*B*).

The apparent strengths of the associations between GK5 and SREBP-1/-2 were much greater than between GK and SREBP-1/-2 (Fig. S8 *A* and *B*). We also detected an association between stably expressed FLAG-tagged GK5 and endogenous SREBP-1 (precursor), SREBP-2 (both precursor and the processed C-terminal domain), or GK in mouse 3T3-L1 cells (Fig. 7*C*) and in human HepG2 cells (Fig. 7*D*). Experiments in which HA-tagged GK5 or GK and truncated FLAG-tagged SREBP-1 and SREBP-2 were expressed in HEK293T cells demonstrated that the C-terminal regulatory domains of SREBP-1 and SREBP-2 were necessary and sufficient for interaction with GK5 or GK (Fig. 7*E* and Fig. S8*C*). These data suggest that GK5 interacts with SREBP-1 and SREBP-2 in a kinase-independent manner and thereby inhibits their proteolytic processing.

SREBPs use their C-terminal regulatory domain to bind SCAP, an interaction required for the movement of SREBPs to the Golgi apparatus where SREBPs are proteolytically processed. We tested whether the interaction between GK5 and the C-terminal domain of SREBP blocks the binding of the SREBPs to SCAP. As

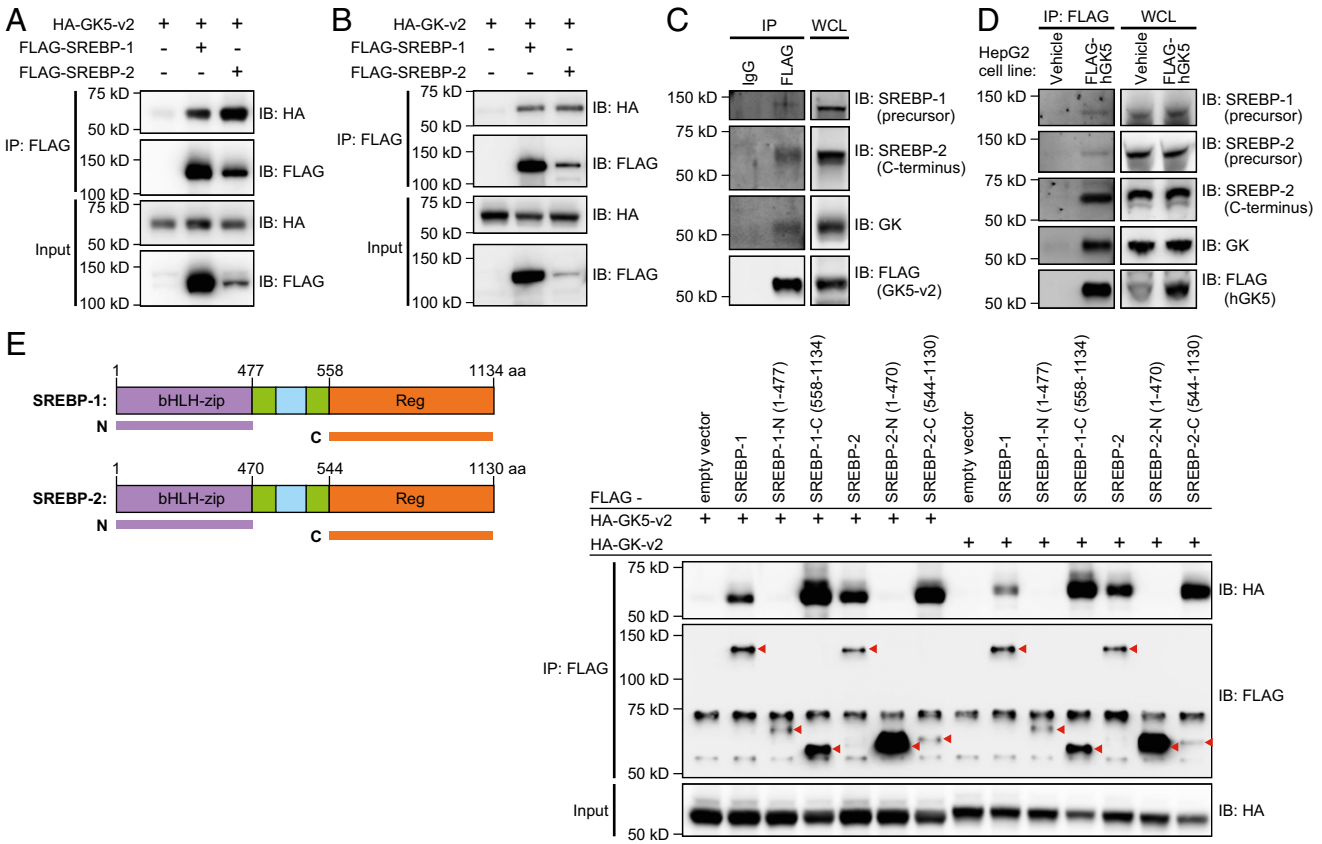

Fig. 7. GK5 and GK bind to the C-terminal regulatory domain of SREBP-1 and SREBP-2. (*A*) HEK293T cells were transfected with HA-tagged GK5-v2 and either FLAG-SREBP-1 or FLAG-SREBP-2. Cell lysates were immunoprecipitated using anti-FLAG M2 agarose and immunoblotted with antibodies against HA or FLAG. (*B*) HEK293T cells were transfected with HA-tagged GK-v2 and either FLAG-SREBP-1 or FLAG-SREBP-2. Cell lysates were immunoprecipitated using anti-FLAG M2 agarose and immunoblotted with antibodies against HA or FLAG. (*C*) 3T3-L1 cells were infected with lentivirus encoding FLAG-tagged GK5-v2. Lysates of the stable cell lines were immunoprecipitated using either anti-FLAG M2 agarose or IgG control agarose and immunoblotted with the indicated antibodies. (*D*) HepG2 cells were infected with lentivirus encoding FLAG-tagged human GK5 (529 amino acids) or empty vector alone (vehicle). Lysates of these two stable cell lines were immunoprecipitated using anti-FLAG M2 agarose and immunoblotted with the indicated antibodies. (*E*) Constructs expressing either the FLAG-tagged N-terminal transcription factor domain (bHLH-zip) or the FLAG-tagged C-terminal regulatory (Reg) domain of SREBP-1 or SREBP-2 were expressed with either a HA-tagged GK5-v2 or a HA-tagged GK-v2. Lysates were subsequently immunoprecipitated using anti-FLAG M2 agarose and immunoblotted using the indicated antibodies.

expected, tagged SREBP-1 or SREBP-2 and SCAP coimmunoprecipitated following coexpression in HEK293T cells (Fig. S9 *A* and *B*). However, the expression of GK5 had no effect on the interaction between SCAP and SREBP-1 (Fig. S9*A*) or between SCAP and SREBP-2 (Fig. S9*B*).

Discussion

We have shown that GK5, a member of the glycerol kinase family, is a component of the regulatory apparatus for cholesterol production mediated by SREBP-1 and SREBP-2 in the skin. GK5 negatively regulates processing of the SREBPs and subsequent cholesterol biosynthesis in skin. Based on its histological location, GK5 probably acts chiefly in sebocytes. Given that increased activation of SREBPs and their target genes was confined to the skin of homozygous *toku* mice, our findings also demonstrate that distinct tissues (at least skin and liver) can independently regulate cholesterol biosynthesis. However, we found that GK5-dependent regulation of SREBPs could be transferred to the embryonic kidney cell line HEK293T by overexpression of GK5, which reduced the amount of transcriptionally active SREBP-2 in the nuclear fraction of these cells.

Both deficiency and overabundance of cholesterol are associated with alopecia and skin defects in mice and humans carrying mutations in enzymes of the cholesterol biosynthetic pathway and in transcription factors regulating lipid metabolism (31, 34, 35). These proteins include the enzymes 3β-hydroxysteroid-Δ7-reductase (DHCR7), sterol C-5-desaturase (SC5D), and sterol-Δ8-Δ7-isomerase (encoded by *EBP*); the regulatory proteins Insig-1 and Insig-2; and the transcription factor peroxisome proliferator-activated receptor γ (PPARγ); mutations in each of these proteins also results in accumulation of one or more of the sterol precursors of cholesterol. Therefore, the accumulation of sterol precursors rather than aberrant cholesterol levels per se may be causative for the hair growth defects in these instances (29, 31). The reversal of alopecia by simvastatin treatment of $Gk5^{toku/toku}$ mice supports the idea that the buildup of sterol precursors is detrimental to hair follicle development and homeostasis. Similarly, accumulation of HMGCR and sterol precursors in the skin, hair follicle degeneration, and alopecia observed in Epi-*Insig*-DKO mice, which lack Insig-1 and Insig-2 expression in the epidermis, were rescued by simvastatin treatment (31).

The enzymatic function of GK is to catalyze ATP-dependent phosphorylation of glycerol to form glycerol-3-phosphate, which is used in gluconeogenesis and lipid synthesis. GK5 also exhibited glycerol kinase activity in vitro, and up-regulation of GK expression such that total glycerol kinase activity was normal in the skin of *toku* homozygous mice suggested that this enzymatic activity is biologically important. Moreover, GK and GK5 were found to bind to each other, possibly indicating that they can function as a heterodimer, similar to bacterial forms of

GK that function as homodimers (36). The observation of hair loss in $Gk5^{D280N/D280N}$ mice, which express a kinase-inactive but otherwise intact GK5 protein, confirmed the importance of GK5 kinase activity for hair growth. However, the physiological substrate, the phosphorylation of which is necessary, remains unknown; an in vitro kinase assay suggested that it is not SREBP-1/-2 (Fig. S7*B*), and normal levels of skin glycerol kinase activity in *toku* homozygotes suggested that it is not glycerol (Fig. 2*F*).

We observed increased accumulation of the proteolytically processed SREBP-1/-2 N-terminal bHLH-ZIP domain in the nuclei of *toku* homozygous skin. However, based on the exclusive localization of GK5 in the cytoplasm and its failure to interact with the N-terminal bHLH-ZIP domain of SREBP-1/-2, we proposed that elevated nuclear accumulation of processed SREBPs originates from increased proteolytic processing rather than from augmented nuclear translocation. Following from this, we hypothesized that the interaction between GK5 and SREBP-1/-2 may prevent the binding of the SREBPs to SCAP, thereby inhibiting SREBP translocation to the Golgi and subsequent processing, but this was not evident from coimmunoprecipitation experiments. Given this finding and the requirement for GK5 kinase activity for hair growth, it seems unlikely that regulation of SREBPs is mediated by direct interaction with GK5. Further work is necessary to elucidate the mechanistic link between GK5 and SREBPs, which may entail crosstalk between the glycerol metabolism pathway and the cholesterol biosynthesis pathway. To date, the regulation of SREBPs in sebocytes remains unexplained, although it does not appear to involve control by C/EBPα (37).

More than 2,800 polymorphisms in human *GK5* have been reported. Although minor allele frequencies are not available for most reported polymorphisms, 11 variants have minor allele frequencies less than 0.5%. We speculate that such rare variants may in some cases be associated with inherited alopecia manifested in infancy or childhood.

Materials and Methods

Mice. C57BL/6J mice purchased from The Jackson Laboratory were mutagenized with ENU as described (38). Mice were maintained at the University of Texas Southwestern Medical Center, and all husbandry and experiments were performed in accordance with protocols approved by the Institutional Animal Care and Use Committee. Mouse strain and genotyping information are in *SI Materials and Methods*.

Generation of Mice with Targeted Mutations. TALEN- or CRISPR-Cas9–mediated gene targeting were used to generate $Gk5^{-/-}$, $Gk2^{-/-}$, and $Gk5^{D280N/D280N}$ mice, as described in *SI Materials and Methods*.

Genetic Mapping of the *toku* Mutation. The *toku* phenotype was mapped by bulk segregation analysis (39) to mouse chromosome 9 using 15 affected and 32 unaffected F2 mice from intercrosses of B6/B10 F1 hybrids, to a critical region on chromosome 9 delimited by markers B10SNPS0141 and B10SNPS0147 at 65,069,297 and 122,496,139 bp (NCBI m37), respectively. Fine mapping using 68 affected and 179 unaffected F2 mice narrowed down the critical region to 6.8 Mbp (92,626,213–99,422,251 bp). *Esyt3* and *Gk5* were selected for Sanger sequencing from more than 15 genes located in the critical region because expression levels in mouse skin were predicted by BioGPS (Dataset: GeneAtlas MOE430, gcrma) to be high.

The *toku* mutation was confirmed and the mutations in the *barrener* and *tangyuan* strains were mapped using the Illumina HiSEq. 2500 platform. Whole-exome sequencing and mapping were performed as described (40). The effect of the *toku*, *barrener*, and *tangyuan* mutations were predicted by using the HumDiv-trained PolyPhen-2 server (version 2.2.2) (41).

Skin Grafts. Skin grafts were performed as described (42). Recipient mice were anesthetized and hair around the chest was shaved with surgical blades. The graft bed was prepared on the dorsal region under aseptic conditions. The graft bed was prepared by carefully removing the epidermis and dermis to the level of the panniculus carnosus without disturbing the vascular bed. Donor thoracic skin was prepared in the same manner, i.e., removing the epidermis and dermis and placing in a sterile petri dish wetted with PBS. The donor skin was then placed into the recipient vascular bed and a 1- to 2-mm margin was left on all sides. The grafted skin was covered with sterile, antibiotic (bacitracin)-impregnated Vaseline gauze, covered with a bandage, and then wrapped in cloth tape. The grafts were left undisturbed for 7 d. On day 7, the bandages were removed, and the grafts were photographed daily.

Plasmids. cDNA of GK5 was subcloned into pBOB lentivector and pcDNA6 vector with C-terminal FLAG or 3xHA tags. cDNAs of GK and SCAP were subcloned into pcDNA6 vector with N-terminal tags. SREBP-1 and SREBP-2 were amplified from the Addgene plasmids (#32017 and #32018, respectively) and subcloned into pcDNA6 vector with N-terminal tags. Domains and fragments of GK5, GK, and SREBPs were cloned in the same way as full-length cDNA. Subcloning was performed using the In-Fusion HD Cloning kit (Clontech). All plasmids were verified by DNA sequencing.

Immunoprecipitation, Immunoblotting, and Antibodies. Immunoprecipitation and immunoblotting were performed according to standard procedures as described in *SI Materials and Methods*. Anti-GK5 polyclonal antibody was raised in rabbits using an *E. coli*-expressed GST-GK5 peptide (amino acids 2–72 of mouse GK5) and subsequently purified using antigen-affinity chromatography. Other antibodies and their sources are listed in *SI Materials and Methods*.

Cytoplasmic-Nuclear Fractionation. To prepare cytoplasmic and nuclear extracts from the skin, cytoplasmic-nuclear fractionation was performed using the Subcellular Protein Fractionation Kit for Tissues (Thermo Fisher). Five fractions were made according to the manufacturer's protocol (cytoplasmic extract, membrane extract, soluble nuclear extract, chromatin-bound extract, and cytoskeletal extract). Total nuclear fraction was prepared by mixing matched soluble nuclear extract and chromatin-bound extract. To prepare cytoplasmic and nuclear extracts from the cultured cells, cytoplasmic-nuclear fractionation was performed using the NE-PER Nuclear and Cytoplasmic Extraction Reagents (Thermo Fisher).

RNA Extraction and qRT-PCR. RNA extraction and qRT-PCR were performed according to standard procedures as described in *SI Materials and Methods*.

Histology, Immunohistochemistry, and Immunofluorescence. Skin from the upper back was collected from mice at P10, P16, P21, and P28. For routine histology, special stains, and immunohistochemistry (IHC), specimens were harvested and fixed or cryoembedded according to standard procedures with modifications for tissue type and stains (43, 44). Skin samples were either immersion-fixed in 10% (vol/vol) neutral-buffered formalin for 48 h before storage in 70% (vol/vol) ethanol or cryoembedded in gum tragacanth without fixation. Skin was paraffin-processed, and serial sections were prepared with H&E. GK5, loricrin, keratin 10, and keratin 14 IHC was performed on paraffin-embedded sections with antigen retrieval by microwaving in citra buffer (Biogenex). For loricrin, keratin 10, and keratin 14, the IHC signals were detected using biotinylated secondary antibodies and a fluorescein avidin D cell sorter (Vector Labs). DAPI (Sigma-Aldrich) was used for nuclear counterstain in the fluorescence microscopy. For GK5 IHC, the bound primary was detected using biotinylated goat anti-rabbit secondary antibody and streptavidin-peroxidase (Vector Labs), the color was developed with diaminobenzidine chromogen (Dako), and hematoxylin (Sigma-Aldrich) was used for counterstain. For cellular staining of GK5, a plasmid encoding C-terminal FLAG-tagged GK5 (FLAG-GK5) was transfected into NIH 3T3 cells. Twenty-eight hours later, immunofluorescence was performed using a FLAG antibody (Sigma-Aldrich) and Alexa Fluor-conjugated secondary antibody (Thermo Fisher). Nuclei were stained with DAPI.

Measurement of Glycerol Kinase Activity. Full-length GK5 with an N-terminal MBP tag was expressed in *E. coli*. The MBP moiety was removed by TEV protease, and the GK5 protein was purified by fast protein liquid chromatography. Purified recombinant protein was analyzed by SDS/PAGE gel and Coomassie Blue Staining (Thermo Fisher). The glycerol kinase activity of the GK5 protein was determined by a kinase assay kit (R&D Systems) per manufacturer's instructions using glycerol as the substrate. The positive control for this assay was recombinant *E. coli* glycerol kinase (glpK) from R&D Systems.

Back skins, livers, and kidneys were harvested from *toku* and wild-type mice, homogenized, and lysed in Nonidet P-40 lysis buffer. To remove the detergents that might affect kinase activity in the samples, the supernatants were desalted using PD-10 desalting columns (GE Healthcare Life Sciences), and the buffer was exchanged to Tris-buffered saline (25 mM Tris–Cl, pH 7.8, 150 mM NaCl; the isoelectric point of GK5 is 6.84). The protein concentrations

were determined by bicinchoninic acid (BCA) protein assay. The kinase activity in the total lysates was determined as above.

Lipid Analysis by LC-MS/MS. Skin lipids were extracted by immersing the whole mouse in acetone for 3 min. The solvent was then dried in nitrogen gas in a 40 °C water bath. For the analysis of lipid samples, liquid chromatography coupled with high-resolution mass spectrometry was used as detailed in *SI Materials and Methods*.

Measurement of Free Cholesterol, Cholesteryl Esters, or Both (Total Cholesterol) in the Skin and Serum. Free cholesterol, cholesteryl esters, and total cholesterol in the skin and in the sera were determined using a Cholesterol Quantitation Kit (Sigma-Aldrich). In brief, age-matched *toku* and wild-type mice (~3 mo old) were bled (for sera) and then euthanized. Skin lipids were extracted by soaking the mice in acetone for 1 min. The acetone solutions were centrifuged at 3,000 × *g* for 15 min to remove insoluble materials. A 1-mL aliquot of each supernatant was taken and vacuum-dried. The dried lipids were then dissolved by adding 500 μL of the cholesterol assay buffer from the kit, followed by vortex and sonication until the mixture was homogenous. The lipid solutions and sera were used for cholesterol quantitation using the kit per manufacturer's instructions.

Simvastatin Treatment of the *toku* Homozygotes. Simvastatin treatment was performed according to ref. 31 with slight modifications. A simvastatin stock solution of 6.4 mg/mL in propylene glycol/ethanol (PG/E) was prepared by dissolving 400 mg of simvastatin (Merck Millipore) in 8 mL of ethanol at 70 °C and converting it to its active hydroxyl acid form by the addition of 2 mL of 0.6 N NaOH. The resulting solution was titrated to pH 7.4, and PG (Sigma-Aldrich) was added to give a final PG/E ratio of 7:3 (vol/vol). The back skin of each mouse was rubbed for 30 s with an acetone-soaked cotton swab to make the skin permeable. Immediately thereafter, 156 μL of the simvastatin solution or PG/E solvent (control) was applied to the acetone-treated area. These treatments were carried out daily from P2 to P14, and the mice were photographed at 3 mo.

In Vitro GK5 kinase Assay. Kinase activity of recombinant GK5 toward SREBP-1/-2 was measured as described in *SI Materials and Methods*.

Statistical Analysis. The statistical significance of the differences between two groups was determined using the two-tailed Student's *t* test. Where relevant, the *P* values are indicated on the figures. Differences with $P < 0.05$ were considered statistically significant.

ACKNOWLEDGMENTS. We thank Drs. Joseph L. Goldstein and Guosheng Liang for useful suggestions and SREBP antibodies; Dr. Hong Zhang for help with the prediction of amino acid residues required for GK5 kinase activity; and Peter Jurek for his expert assistance with the figures. This work was supported by NIH Grant U19 AI100627.

1. Krause MR, Regen SL (2014) The structural role of cholesterol in cell membranes: From condensed bilayers to lipid rafts. *Acc Chem Res* 47:3512–3521.
2. Elias P, Feingold K, Fartasch M (2006) *Skin Barrier*, eds Elias P, Feingold K (Taylor & Francis, New York), pp 261–272.
3. Elias PM, et al. (1984) Stratum corneum lipids in disorders of cornification. Steroid sulfatase and cholesterol sulfate in normal desquamation and the pathogenesis of recessive X-linked ichthyosis. *J Clin Invest* 74:1414–1421.
4. Feingold KR, et al. (1990) Cholesterol synthesis is required for cutaneous barrier function in mice. *J Clin Invest* 86:1738–1745.
5. Feingold KR (2009) The outer frontier: The importance of lipid metabolism in the skin. *J Lipid Res* 50:S417–S422.
6. Feingold K, Elias P (2014) The important role of lipids in the epidermis and their role in the formation and maintenance of the cutaneous barrier. *Biochim Biophys Acta* 1841:279.
7. Gray GM, White RJ, Williams RH, Yardley HJ (1982) Lipid composition of the superficial stratum corneum cells of pig epidermis. *Br J Dermatol* 106:59–63.
8. van Smeden J, Janssens M, Gooris GS, Bouwstra JA (2014) The important role of stratum corneum lipids for the cutaneous barrier function. *Biochim Biophys Acta* 1841:295–313.
9. Niemann C, Horsley V (2012) Development and homeostasis of the sebaceous gland. *Semin Cell Dev Biol* 23:928–936.
10. Greene RS, Downing DT, Pochi PE, Strauss JS (1970) Anatomical variation in the amount and composition of human skin surface lipid. *J Invest Dermatol* 54:240–247.
11. Zouboulis CC, et al. (2008) Frontiers in sebaceous gland biology and pathology. *Exp Dermatol* 17:542–551.
12. Lee WS (2011) Integral hair lipid in human hair follicle. *J Dermatol Sci* 64:153–158.
13. Picardo M, Ottaviani M, Camera E, Mastrofrancesco A (2009) Sebaceous gland lipids. *Dermatoendocrinol* 1:68–71.
14. Georgel P, et al. (2005) A toll-like receptor 2-responsive lipid effector pathway protects mammals against skin infections with gram-positive bacteria. *Infect Immun* 73:4512–4521.
15. Ye J, DeBose-Boyd RA (2011) Regulation of cholesterol and fatty acid synthesis. *Cold Spring Harb Perspect Biol* 3:a004754.
16. Yokoyama C, et al. (1993) SREBP-1, a basic-helix-loop-helix-leucine zipper protein that controls transcription of the low density lipoprotein receptor gene. *Cell* 75:187–197.
17. Sharpe LJ, Brown AJ (2013) Controlling cholesterol synthesis beyond 3-hydroxy-3-methylglutaryl-CoA reductase (HMGCR). *J Biol Chem* 288:18707–18715.
18. Hua X, Wu J, Goldstein JL, Brown MS, Hobbs HH (1995) Structure of the human gene encoding sterol regulatory element binding protein-1 (SREBF1) and localization of SREBF1 and SREBF2 to chromosomes 17p11.2 and 22q13. *Genomics* 25:667–673.
19. Deng X, et al. (2002) Regulation of the rat SREBP-1c promoter in primary rat hepatocytes. *Biochem Biophys Res Commun* 290:256–262.
20. Deng X, et al. (2007) Expression of the rat sterol regulatory element-binding protein-1c gene in response to insulin is mediated by increased transactivating capacity of specificity protein 1 (Sp1). *J Biol Chem* 282:17517–17529.
21. Horton JD, et al. (2003) Combined analysis of oligonucleotide microarray data from transgenic and knockout mice identifies direct SREBP target genes. *Proc Natl Acad Sci USA* 100:12027–12032.
22. Pai JT, Guryev O, Brown MS, Goldstein JL (1998) Differential stimulation of cholesterol and unsaturated fatty acid biosynthesis in cells expressing individual nuclear sterol regulatory element-binding proteins. *J Biol Chem* 273:26138–26148.
23. Goldstein JL, DeBose-Boyd RA, Brown MS (2006) Protein sensors for membrane sterols. *Cell* 124:35–46.
24. Sun LP, Li L, Goldstein JL, Brown MS (2005) Insig required for sterol-mediated inhibition of Scap/SREBP binding to COPII proteins in vitro. *J Biol Chem* 280:26483–26490.
25. Horton JD, Goldstein JL, Brown MS (2002) SREBPs: Activators of the complete program of cholesterol and fatty acid synthesis in the liver. *J Clin Invest* 109:1125–1131.
26. Gasic GP (1994) Basic-helix-loop-helix transcription factor and sterol sensor in a single membrane-bound molecule. *Cell* 77:17–19.
27. Wang X, Sato R, Brown MS, Hua X, Goldstein JL (1994) SREBP-1, a membrane-bound transcription factor released by sterol-regulated proteolysis. *Cell* 77:53–62.
28. Wu C, et al. (2009) BioGPS: An extensible and customizable portal for querying and organizing gene annotation resources. *Genome Biol* 10:R130.
29. Stenn KS, Karnik P (2010) Lipids to the top of hair biology. *J Invest Dermatol* 130:1205–1207.
30. Goldstein JL, Brown MS (1990) Regulation of the mevalonate pathway. *Nature* 343:425–430.
31. Evers BM, et al. (2010) Hair growth defects in Insig-deficient mice caused by cholesterol precursor accumulation and reversed by simvastatin. *J Invest Dermatol* 130:1237–1248.
32. Osborne TF (2001) CREating a SCAP-less liver keeps SREBPs pinned in the ER membrane and prevents increased lipid synthesis in response to low cholesterol and high insulin. *Genes Dev* 15:1873–1878.
33. Rahib L, MacLennan NK, Horvath S, Liao JC, Dipple KM (2007) Glycerol kinase deficiency alters expression of genes involved in lipid metabolism, carbohydrate metabolism, and insulin signaling. *Eur J Hum Genet* 15:646–657.
34. Herman GE (2003) Disorders of cholesterol biosynthesis: Prototypic metabolic malformation syndromes. *Hum Mol Genet* 12:R75–R88.
35. Karnik P, et al. (2009) Hair follicle stem cell-specific PPARgamma deletion causes scarring alopecia. *J Invest Dermatol* 129:1243–1257.
36. Yeh JI, et al. (2004) Structures of enterococcal glycerol kinase in the absence and presence of glycerol: Correlation of conformation to substrate binding and a mechanism of activation by phosphorylation. *Biochemistry* 43:362–373.
37. Harrison WJ, Bull JJ, Seltmann H, Zouboulis CC, Philpott MP (2007) Expression of lipogenic factors galectin-12, resistin, SREBP-1, and SCD in human sebaceous glands and cultured sebocytes. *J Invest Dermatol* 127:1309–1317.
38. Hoebe K, Du X, Goode J, Mann N, Beutler B (2003) *Lps2*: A new locus required for responses to lipopolysaccharide, revealed by germline mutagenesis and phenotypic screening. *J Endotoxin Res* 9:250–255.
39. Xia Y, et al. (2010) Bulk segregation mapping of mutations in closely related strains of mice. *Genetics* 186:1139–1146.
40. Wang T, et al. (2015) Real-time resolution of point mutations that cause phenovariance in mice. *Proc Natl Acad Sci USA* 112:E440–E449.
41. Adzhubei IA, et al. (2010) A method and server for predicting damaging missense mutations. *Nat Methods* 7:248–249.
42. Mayumi H, Nomoto K, Good RA (1988) A surgical technique for experimental free skin grafting in mice. *Jpn J Surg* 18:548–557.
43. Sheehan DC, Hrapchak BB (1980) *Theory and Practice of Histotechnology* (Battelle Press, Columbus, OH).
44. Woods AE, Ellis RC (1996) *Laboratory Histopathology: A Complete Reference* (Churchill Livingstone, New York).
45. Sanjana NE, et al. (2012) A transcription activator-like effector toolbox for genome engineering. *Nat Protoc* 7:171–192.